

1 **The changing character of twenty-first century precipitation over the**
2 **western United States in the variable-resolution CESM**

3 Xingying Huang, * Paul A. Ullrich

4 *Department of Land, Air and Water Resources, University of California, Davis*

5 *Corresponding author address: Xingying Huang, Department of Land, Air and Water Resources,
6 University of California Davis, Davis, CA 95616.
7 E-mail: xyhuang@ucdavis.edu

ABSTRACT

8 (To be added once the main content settled down)

9 **1. Introduction**

10 There is substantial and growing interest in understanding the character of precipitation within
11 a changing climate, in large part because of the pronounced impacts of water availability on
12 socioeconomic and natural systems (Hegerl et al. 2004; Kharin et al. 2007; Scoccimarro et al.
13 2013). Among these studies, precipitation extremes have been a major focus, particularly drought
14 and flood events (Seneviratne et al. 2012). Studies examining the character of precipitation in a
15 warming world, which utilize models of varying complexity, from simple thermodynamic models
16 through complex coupled climate simulations, suggest that although atmospheric water vapor is
17 increasing, the consequences for precipitation are far more complicated. Extreme precipitation
18 events are particularly nuanced: Our best projections suggest that extreme precipitation events
19 will intensify even in regions where mean precipitation decreases (Tebaldi et al. 2006; Kharin
20 et al. 2007).

21 Although future climate projections are subject to large uncertainties, climate models are
22 nonetheless one of the most versatile tools for studying climate variability and extremes events
23 in the future (Easterling et al. 2000). Global climate models (GCMs) have often been used to
24 investigate changes in the mean, variability and extremes of climate, as forced with predicted
25 greenhouse gas (GHGs) concentrations and aerosol emissions (Meehl et al. 2006). Several past
26 studies have investigated global impacts (Seneviratne et al. 2012), but studies addressing impacts
27 at local and regional scales are less common. Although increased GHG concentrations have con-
28 tributed to the observed intensification of heavy precipitation events over the tropical ocean (Allan
29 and Soden 2008) and the majority of Northern Hemisphere overland areas Min et al. (2011), these
30 impacts are much more poorly understood at regional scales due to variability at finer spatial scales
31 associated with the atmospheric circulation (Trenberth 2011). As a consequence of this variability,

³² a confident assessment of changes in regional extremes requires both high spatial resolution and
³³ a long integration period, both of which can make the computational cost untenable for global
³⁴ simulations.

³⁵ This issue of insufficient regional-scale climate information has been a major outstanding prob-
³⁶ lem in climate science, as stakeholders and water managers typically require fine-scale information
³⁷ on climate impacts in order to effectively develop adaptation and mitigation strategies. Dynami-
³⁸ cal downscaling with regional climate models (RCMs) has been one of the few tools available to
³⁹ ascertain the frequency, intensity, and duration of extreme events at the needed scales. By only
⁴⁰ simulating a limited regional domain, RCMs better capture fine-scale dynamical features with
⁴¹ high horizontal resolution (Bell et al. 2004; Frei et al. 2006; Rauscher et al. 2010; Wehner 2013).

⁴² Higher resolution enables more accurate simulation of precipitation extremes, which are driven
⁴³ by land use, land/water contrast, snow cover, cloudiness and circulation patterns associated with
⁴⁴ topography (Leung et al. 2003a; Diffenbaugh et al. 2005; Salathé Jr et al. 2008; Wehner et al.
⁴⁵ 2010). Diffenbaugh et al. (2005) studied both heat events and wet events over the contiguous
⁴⁶ United States using a RCM configured at 25 km horizontal resolution, and demonstrated that fine-
⁴⁷ scale processes were critical for accurate assessment of local- and regional-scale climate change
⁴⁸ vulnerability. Leung et al. (2003b) showed that the higher-resolution RCMs yield more realis-
⁴⁹ tic precipitation patterns and produce more frequent heavy precipitation over the western U.S.
⁵⁰ (WUS), consistent with observations.

⁵¹ Despite their success, RCMs also have known issues associated with inconsistency between
⁵² the lateral forcing data and the driven RCM. The menu of physical parameterizations and tuning
⁵³ parameters typically available to RCMs can also lead to over-tuning of the model for a partic-
⁵⁴ ular geographic region or climatological field (McDonald 2003; Laprise et al. 2008; Mesinger
⁵⁵ and Veljovic 2013). Consequently, there has been growing interest in variable-resolution enabled

56 GCMs (VRGCMs) to improve regional climate simulations. Unlike RCMs, which require GCM
57 data to drive the simulation at lateral boundaries, VRGCMs use a unified model with coarse global
58 resolution and enhanced resolution over a specific study region (Staniforth and Mitchell 1978;
59 Fox-Rabinovitz et al. 1997). VRGCMs have demonstrated competitive ability for regional climate
60 studies at a reduced computational cost, particular when compared to uniform-resolution GCMs
61 (Fox-Rabinovitz et al. 2006; Rauscher et al. 2013).

62 In this paper, we utilize the recently developed variable-resolution option in the Community
63 Earth System Model (VR-CESM). VR-CESM is based on the CESM (and its predecessor, the
64 Community Climate System Model (CCSM)), a family of models that have been used for decades
65 to study the global climate (Neale et al. 2010a; Hurrell et al. 2013). The overall performance of
66 VR-CESM for modeling regional climate in the California and Nevada is detailed in Huang et al.
67 (2016), where it was argued that VR-CESM has competitive biases in comparison to the Weather
68 Research and Forecasting (WRF) model (a traditional RCM) and the uniform-resolution CESM,
69 when evaluating both against high-quality observations and reanalysis. VR-CESM has been used
70 in a number of studies to simulate fine-scale atmospheric processes (Zarzycki et al. 2014, 2015;
71 Rhoades et al. 2015).

72 This study focuses on changes in the character of precipitation over the 21st Century within the
73 WUS, as predicted from long-term ensemble runs conducted with VR-CESM with a local grid
74 resolution of $\sim 0.25^\circ$. The WUS is known to be particularly vulnerable to hydrological extremes,
75 particularly floods and droughts (Leung et al. 2003b; Caldwell 2010), and hosts a variety of local
76 features and microclimates associated with its rough and varied topography. Simulations of the fu-
77 ture climate are performed in accordance with the representative concentration pathway (RCP) 8.5
78 scenario, which describes a “business-as-usual” projection for GHGs (Riahi et al. 2011). RCP8.5
79 is a baseline scenario with updated base year calibration (to 2005) and no explicit climate policy. In

80 this study we focus on a single RCP since end-of-century projections with the substantially more
81 optimistic RCP2.6 scenario have been found to be qualitatively similar to mid-century RCP8.5
82 results (which are assessed in this study). Simulations are further conducted in accordance with
83 the Atmospheric Model Intercomparison Project (AMIP) protocol (Gates 1992), a widely-used
84 approach for climate model diagnosis, validation and intercomparison that imposes global sea sur-
85 face temperatures (SSTs) and sea ice. It is well-known that correctly simulating changes to the
86 spatial pattern of SSTs in state-of-the-art coupled GCMs remains a significant challenge (Joseph
87 and Nigam 2006; Stevenson 2012; Jha et al. 2014; Taschetto et al. 2014). However, by constraining
88 atmospheric boundary conditions at the sea surface, we avoid model biases that are known to exist
89 in the fully coupled configuration (Grodskey et al. 2012; Small et al. 2014) and accept potential
90 uncertainties associated with our choice of SSTs.

91 Changes in the character of precipitation, in terms of frequency and intensity, have been assessed
92 in our study from recent history through the end of 21st century. A comprehensive set of metrics
93 for precipitation extremes have been evaluated from ensemble simulations over the 26-year peri-
94 ods corresponding to historical (1980-2005), mid-century (2025-2050) and end-of-century (2075-
95 2100). We hypothesize that spatial inhomogeneity in local geography and temperature will also
96 result in similarly inhomogeneous impacts on the precipitation field. We further expect that tele-
97 connections (specifically the El Niño-Southern Oscillation, ENSO) will have a pronounced impact
98 on precipitation features. Since only one SST dataset was used for this study, we note that our
99 projections are conditioned on a particular future character of ENSO. This is a potentially large
100 source of uncertainty, as at present there is no clear consensus on how ENSO may behave under a
101 warming climate (Fedorov and Philander 2000; Latif and Keenlyside 2009; Guilyardi et al. 2009;
102 Collins et al. 2010; DiNezio et al. 2012), and strengthening or weakening of this pattern will have
103 clear consequences for our results (as discussed in section 6d).

104 This work builds on a number of previous studies that have explored the projected future change
105 in WUS precipitation. For example, Kim (2005) applied downscaled climate change signals to se-
106 lected indicators, and concluded that global warming induced by increased CO₂ is likely to drive
107 increases in extreme hydrologic events in the WUS. Duffy et al. (2006) found that changes to
108 mean precipitation predicted by the RCMs are not statistically significant compared to interannual
109 variability in many regions over WUS, although there is little consistency among the different
110 RCMs as to responses in precipitation to increased GHGs. Gao et al. (2015) pointed out a poten-
111 tially large increase in atmospheric river events by the end of the 21st century under the RCP8.5
112 scenario, with implications for large-scale and heavy precipitation events along the Pacific coast.

113 This paper is structured as follows. Section 2 describes the model setup. Section 3 describes
114 the methodology and reference datasets employed. An assessment of the ability of the model to
115 capture the climatology of the WUS is given in section 4. Results from the future mean climato-
116 logical trend and projected changes to precipitation indices are in section 6. Section 7 summarizes
117 the main points of the study along with further discussion.

118 2. Model Setup

119 CESM is a state-of-the-art Earth modeling framework, consisting of coupled atmosphere, ocean,
120 land and sea ice models (Neale et al. 2010b; Hurrell et al. 2013). In this study, the Community At-
121 mosphere Model version 5 (CAM5) (Neale et al. 2010b) and the Community Land Model version
122 4.0 (Oleson et al. 2010) are used. CAM5 is configured with the Spectral Element (SE) dynamical
123 core, which is known for its conservation properties, accuracy and parallel scalability (Dennis et al.
124 2011; Taylor 2011) and incorporates the variable-resolution option (Zarzycki et al. 2014). CLM
125 is employed in the *unigrid* configuration, which allows the land model and atmospheric model to
126 utilize the same model grid so eliminates the need for interpolation. SSTs and sea ice, which are

127 used to compute ocean-atmosphere fluxes, are prescribed in accordance with the AMIP protocol
128 (Gates 1992). The variable-resolution mesh used for this study is depicted in Figure 1, in accord
129 with our past studies (Rhoades et al. 2015; Huang et al. 2016; Huang and Ullrich 2016).

130 Simulations have been performed for the historical period (1979-2005, hereafter referred to as
131 hist) and for two future periods: 2024-2050 (hereafter referred to as mid) and 2074-2100 (hereafter
132 referred to as end). Daily output are recorded for each period on the native SE grid and then
133 remapped to a regional latitude-longitude mesh (Ullrich and Taylor 2015; Ullrich et al. 2016). For
134 purposes of analysis, the first year of each time period was discarded as a spin-up period to allow
135 adequate time for the initialized land and atmosphere to equilibrate. The 26-year duration was
136 chosen to provide an adequate sampling of annual variability for each time phase. As mentioned
137 earlier, GHG concentrations are set based on RCP8.5. Historical SSTs and sea ice are prescribed
138 at 1° resolution, as described by Hurrell et al. (2008). SSTs and sea ice for each future period are
139 developed from fully-coupled RCP 8.5 climate simulations with bias correction applied (Cecile
140 Hannay, personal communication). Annually-updated land surface datasets, which prescribe land-
141 use characteristics, are interpolated from 0.5° to the land model grid.

142 Ensemble runs are needed to ensure that the sample adequately accounts for climate variability,
143 especially for statistics associated with climatological extremes. However, the exact number of
144 ensemble members required is heavily dependent on the variability of the particular metric being
145 examined, and so no standard ensemble criteria exists. Deser et al. (2012b) suggest that around
146 3 ensemble runs are required to detect a significant epoch difference for JJA (June-July-August)
147 surface temperatures, whereas 10 to 30 ensemble members are needed for that for DJF (Dec.-Jan.-
148 Feb.) precipitation. In our study, the use of prescribed SSTs does reduce the intrinsic variability
149 of the climate system (see supplement), and so we found reasonably converged results with two
150 ensemble members for the historical period and four ensemble members for each future period.

151 **3. Methodology**

152 *a. Precipitation indices*

153 Standard indices have been employed to characterize precipitation (Tebaldi et al. 2006; Zhang
154 et al. 2011; Sillmann et al. 2013). In order to choose a comprehensive (but minimal) set that are
155 informative to stakeholders and water managers, indices from throughout the literature have been
156 assessed. The indices examined include those defined by the Expert Team on Climate Change De-
157 tection and Indices (ETCCDI) (Karl et al. 1999) that are featured in earlier studies (Dulière et al.
158 2011; Sillmann et al. 2013; Diffenbaugh et al. 2005; Singh et al. 2013) and others such as return
159 levels, dry spell and wet spell characteristics defined by either percentiles or by selected thresh-
160 olds. The indices we have chosen for this study attempt to provide a relatively comprehensive
161 characterization of precipitation, and are summarized in Table 1.

162 [Paul: You should probably state at some point why you don't employ drought or dry spell
163 indices]

164 *b. Impacts of ENSO*

165 The impact of ENSO on precipitation is emphasized in our study due to its influence on precipi-
166 tation over a majority of our study area, particularly the southwest U.S. (Cayan et al. 1999; Zhang
167 et al. 2010; Deser et al. 2012a; Yoon et al. 2015). The phase of ENSO (*i.e.* El Niño and La Niña)
168 is identified each year using the Oceanic Niño Index (ONI), defined as the 3-month running means
169 of SST anomalies in the Niño 3.4 region (covering 5N-5S, 120-170W based on NOAA (2013)).
170 An El Niño or La Niña episode is said to occur when the ONI exceeds +0.5 or -0.5 for at least five
171 consecutive months for a water year (*i.e.* from July to June) (NOAA 2013) (see the supplement).
172 In order to adjust for the trend in the SST field associated with climate change, the anomaly is

173 computed against the detrended mean SSTs from the periods 1971-2000, 2020-2050 and 2070-
174 2100 for `hist`, `mid` and `end` respectively, using the aforementioned observed and predicted SST
175 datasets. As argued by Kao and Yu (2009), it may be desirable to use an extended Niño 3.4 region
176 to determine the phase of ENSO – however, when employing SST anomalies integrated over the
177 region 105-170W, we observed no significant impact on ONI statistics.

178 *c. Assessing statistical significance*

179 Student's t-test has been used to determine whether or not two datasets at each grid point are
180 statistically equivalent, if the sample population can be adequately described by a normal distri-
181 bution. The normality of a dataset is assessed under the Anderson-Darling test. When the sample
182 populations do not approximately follow a normal distribution, Mann-Whitney-Wilcoxon (MWW)
183 test is employed in lieu of the t-test. All these tests are evaluated at the 0.05 (α) significance level.
184 When comparing different time periods, statistical tests are conducted by treating all years from
185 all ensemble members as independent samples (26×2 sample years for `hist` and 26×4 sample
186 years for `mid` and `end`).

187 (add description of the supplement like what are included; see the `sst_enso.pdf`, mask the land
188 (over land, it should be the surface temperature.))

189 *d. Reference datasets*

190 Gridded observational datasets and reanalysis of the highest available quality, with comparable
191 horizontal resolutions to our VR-CESM simulations, are used for assessing the simulation qual-
192 ity. Multiple reference datasets are necessary due to the underlying uncertainty in interpolating
193 precipitation fields. The three datasets employed are as follows:

194 **UW Gridded Data:** The 0.125° UW daily gridded meteorological data is obtained from
195 the Surface Water Modeling group at the University of Washington, covering the period
196 1949-2010 (Maurer et al. 2002; Hamlet and Lettenmaier 2005). The UW dataset imposes
197 topographic corrections by forcing the long-term average precipitation to match that of the
198 Parameter-elevation Regressions on Independent Slopes Model (PRISM) dataset.

199 **National Centers for Environmental Prediction (NCEP) Climate Prediction Center**
200 **(CPC):** The 0.25° CPC daily dataset provides gauge-based analysis of daily precipitation cov-
201 ering the period 1948-2006. It is a unified precipitation product that covers the Conterminous
202 United States and amalgamates a number of data sources at CPC via optimal interpolation
203 objective analysis.

204 **North American Regional Reanalysis (NARR):** NARR is a ~ 32 km high-resolution reanal-
205 ysis product with 3-hourly output produced by NCEP via dynamical downscaling over North
206 America and covering the period 1979-present (Mesinger et al. 2006).

207 **4. Model Assessment**

208 Before proceeding, we assess the ability of VR-CESM to represent the character of precipitation
209 over the WUS. The indices defined in Table 1 are depicted in Figures 2, 3 and 4 for VR-CESM
210 and each of the reference datasets over the historical period (1980-2005). We assume equal con-
211 fidence in each of the reference datasets, and use Student's t-test (with UW, CPC and NARR as
212 the three statistical samples) to identify regions where VR-CESM deviates significantly from the
213 reference mean. Regions where differences are statistically significant in the VR-CESM dataset
214 are identified with stippling.

215 Overall, VR-CESM largely captures the spatial patterns of precipitation and its indices. As ex-
216 pected, the majority of precipitation is distributed along the northwest coastal area and the moun-
217 tainous regions of the Cascades and the Sierra Nevada. Nonetheless, several apparent biases are
218 present:

219 First, VR-CESM significantly overestimates Pr over dry regions with differences between 0.2
220 mm to 1.5 mm, and over the eastern flank of the Cascades and on both sides of the Sierra Nevada
221 (with relative differences reaching 50%-150%). As with many regional models, VR-CESM is
222 “dreary” and exhibits too many precipitation days (R_{1mm} , $Pr \geq 1$ mm/day and R_{5mm} , 1 mm/day \leq
223 $Pr \leq 5$ mm/day) (see Figure 3) [citation needed]. Nonetheless, over most regions the relative con-
224 tribution of each precipitation frequency subset to total precipitation (F_{1mm} , F_{5mm} , F_{10mm} ,
225 F_{20mm} and F_{40mm}) agrees well, suggesting that the frequency distribution describing precipita-
226 tion intensity is accurately simulated almost everywhere.

227 Second, the spatial pattern of precipitation variability agrees well between VR-CESM and refer-
228 ences with agreement everywhere except in the Great Plains (the eastern edge of our domain) and
229 in California’s Central Valley. The Great Plains is not a focus of this study, but the suppressed vari-
230 ance is primarily during the warm season (April-September) and so likely represents a failure of
231 the convection scheme to adequately simulate variability in this region. This bias is also observed
232 in 0.25° uniform-resolution CESM simulations (Small et al. 2014), and so is not a symptom of the
233 eastern edge of the variable-resolution transition region.

234 However, the grossly exaggerated variability over the western flank of the Sierra Nevada through
235 California’s Central Valley does merit some additional discussion. Here, the overestimation of
236 precipitation and enhanced variability is associated with too many extreme precipitation events
237 ($Pr > 20$ mm/day) (see Figure 4, F_{40mm} and F_{xmm}). This bias is related to exaggerated orographic
238 uplift (upslope winds, not shown) and triggers a dry bias along the eastern flank of the Sierras.

239 Similar biases in simulating extreme precipitation over the topographically complex regions have
240 also been found in high-resolution RCM simulations Walker and Diffenbaugh (2009); Singh et al.
241 (2013), and have been primarily attributed to excessively strong winds. This issue may be further
242 impacted by the diagnostic treatment of precipitation in CAM5 (Morrison and Gettelman 2008;
243 Gettelman et al. 2008).

244 The representation of precipitation in VR-CESM over California was also discussed in Huang
245 et al. (2016), where it was observed that VR-CESM simulations at 0.25° adequately represented
246 regional climatological patterns with high spatial correlation. VR-CESM demonstrated compa-
247 rable performance to WRF at 27 km (which was forced with ERA-Interim reanalysis), but still
248 overestimated overall winter precipitation compared to reference datasets (by about 25%-35%),
249 with the largest differences over the western edge of the Sierra Nevada. This bias is not allevi-
250 ated by simply increasing the spatial resolution, as experimental VR-CESM simulations at 14km,
251 7km and 3.5km show only modest improvement (Alan M. Rhoades, personal communication).
252 This suggests that the bias might be related with more complex dynamic processes rather than
253 treatment of the orographic effects.

254 CESM at 1° resolution was also assessed in order to better understand the impacts of resolution.
255 We find that precipitation patterns over complex topography are poorly represented and do not
256 capture the spatial patterns induced by orographic effects. Over the Cascades and Sierra Nevada,
257 total precipitation grossly underestimated by 1° CESM, when compared to VR-CESM, gridded
258 and reanalysis datasets (see the supplement [[Point to exact figure](#)]). Precipitation has otherwise
259 been smoothed out over the coastal areas and the mountainous regions of the northwest U.S when
260 simulated with CESM at coarse resolution. This result clearly underscores the benefits of high
261 resolution (particularly the representation of topography) in simulating precipitation features. Re-
262 sults are also provided in the supplement for the output from a globally-uniform CESM run at

263 0.25° spatial resolution with the finite volume (FV) dynamical core (Wehner et al. 2014), which
264 exhibits similar performance to VR-CESM (see the supplement [[Point to exact figure](#)]). Overall,
265 0.25° resolution appears to provide the best tradeoff between accuracy and computational cost, as
266 coarser resolution does not correctly represent precipitation features and higher resolution does
267 not appear to substantially improve model accuracy.

268 We have also assessed the impact of the ENSO signal within the historical VR-CESM runs by
269 differencing the precipitation fields between the warm phase (i.e. El Niño) and cool phase (i.e.
270 La Niña), compared to references (see the supplement). ENSO exhibits a weaker signal for obser-
271 vational precipitation, compared to VR-CESM, which might suggest that the model exaggerates
272 ENSO’s impact on precipitation, especially over the northwest U.S. The improvement of ENSO
273 in the model is directly proportional to the representation of ENSO forced precipitation anomalies
274 (AchutaRao and Sperber 2006).

275 **5. Drivers of climatological precipitation change**

276 The remainder of this paper now focuses on model predictions of change over the 21st cen-
277 tury. Precipitation has been observed and modeled to be modified in character at both global and
278 regional scales under climate change. The observed intensification of heavy precipitation events
279 over the recent past for the majority of Northern Hemisphere land areas is primarily attributed
280 to increases in GHGs (Min et al. 2011). GHGs drive radiative changes in the lower troposphere,
281 increase SSTs and lead to increased evaporation, all of which then impact the character of precip-
282 itation events (Allen and Ingram 2002; Sugi and Yoshimura 2004). Several studies have argued
283 that precipitation extremes will intensify continuously through the end of 21st century in both dry
284 and wet regions, although the extent of this change will be spatially heterogeneous (Donat et al.
285 2016).

286 In accordance with the Clausius-Clapeyron (C-C) relationship, saturation vapor pressure in the
287 atmosphere is expected to increase by $\sim 7\%$ for each 1°C increase in temperature (Allan and So-
288 den 2008). As long as a source of water vapor is present, a corresponding increase in atmospheric
289 water vapor content is expected. Naturally, evaporation over the ocean will increase with climate
290 warming, but increases in water vapor content over land may be constrained by soil moisture
291 (Cayan et al. 2010). When specific humidity is high, heavy rain events become more probable,
292 even if total precipitation is decreasing (Trenberth 2011). This suggests that global total precipi-
293 tation is expected to increase at a slower rate than precipitation extremes (Allan and Soden 2008).
294 In accordance with previous studies (e.g. (Allan and Soden 2008; O’Gorman and Schneider 2009;
295 Min et al. 2011)), changes to extreme precipitation follow the C-C relationship more closely than
296 total precipitation amount (Trenberth et al. 2003). However, there is still substantial uncertainty
297 for the magnitude of the change, since precipitation extremes are also dependent on factors such
298 as the vertical velocity profile and temperature (O’Gorman and Schneider 2009).

299 With overland water vapor constrained by soil moisture content, changes to moderate or heavy
300 precipitation events over the WUS are mainly the result of increased large-scale vapor transport
301 from the eastern Pacific Ocean rather than directly from evaporation, typically associated with
302 atmospheric rivers (ARs) and/or orographic uplift (Trenberth et al. 2003; Neiman et al. 2008).
303 Warming may lead to enhancement of the storm track, which would increase ARs along the U.S.
304 west coast with increased air water vapor content in the future (Dettinger 2011; Gao et al. 2015).
305 In the following sections, both the mean changes of precipitation and distributions of both non-
306 extreme and extreme events are investigated as projected by the VR-CESM model under climate
307 forcing.

308 The precipitation of the WUS has strong inter-annual variability caused by large-scale atmo-
309 spheric circulation mainly associated with the ENSO (Leung et al. 2003b). As a significant

310 driver of precipitation, ENSO modulates the storm track behavior over western U.S. with a north-
311 west/southwest precipitation dipole (Gershunov and Barnett 1998), as discussed in d. The pro-
312 jected SSTs we used here states one of the possible cases of ENSO scenarios in the future. How-
313 ever, there is still substantial uncertainty regarding how El Niño will change under global warming
314 (Fedorov and Philander 2000; Guilyardi et al. 2009), which is a source of uncertainty in our results.
315 Capotondi (2013) showed that the diversity of El Niño characteristics in CCSM4 is comparable to
316 what was found in observations, although, as found by Deser et al. (2012c), the overall magnitude
317 of ENSO in CCSM4 [Paul: was this changed at all in CESM1?] is overestimated by 30% over the
318 preindustrial time period.

319 6. Results

320 a. Mean climatology

321 The mean climatological changes in VR-CESM across time periods are depicted in Figure 5.
322 Since the character of WUS precipitation has a strong seasonal contrast, changes to mean precipi-
323 tation, near-surface temperature and near-surface relative humidity are depicted for what we refer
324 to as the cool season (October to March) and the warm season (April to September).

325 As a result of enhanced GHG concentrations, mean annual near-surface temperature (T_{avg})
326 increases by about 1.5 to 2 K from hist to mid and about 4 to 6 K from mid to end. Despite the
327 large spatial variation in mean seasonal temperatures, the observed change to mean temperature is
328 fairly uniform, particularly over the ocean and in coastal regions. Away from the coast there is a
329 weak gradient in the temperature change field, with the largest increase in temperatures occurring
330 towards the northeast during the cool season and towards the north during the warm season. The

331 increase in temperature is also about 0.5K and 1.0K larger during the warm season compared to
332 the cool season for mid and end, respectively.

333 Overall, future RH is constrained closely to hist since it is governed by competing increases in
334 temperature and atmospheric water vapor content. Although RH increases monotonically over the
335 ocean in response to increased evaporation, over land the character is more heterogeneous: In gen-
336 eral, RH tends to increase in regions where Tavg increase is constrained below \sim 2 K, but decrease
337 when Tavg anomaly exceeds \sim 2 K. The decrease in these regions is on the order of 2% and 3-6%,
338 compared to mid and end respectively. In fact, trends in RH are spatially consistent with tempera-
339 ture increase but opposite in magnitude with a spatial correlation coefficient of approximately 0.8.
340 This suggests that continental evaporation and oceanic water vapor transport are insufficient vapor
341 sources when temperature reaches a certain level, consistent with the observation of Joshi et al.
342 (2008). This effect has also been observed in results by Rowell and Jones (2006) over continental
343 and southeastern Europe and Simmons et al. (2010) over low-latitude and midlatitude land areas.

344 In response to these changes to temperature and RH, from hist to mid mean precipitation over
345 the entire domain exhibited a 0.2-0.6 mm/day increase during the cool season. The largest changes
346 were over northwest, where cool-season precipitation emerges from large-scale patterns (namely,
347 atmospheric rivers and associated storm systems)(Trenberth et al. 2003; Neiman et al. 2008). Over
348 the warm season, where precipitation in the WUS is primarily from convection, the increase was
349 around 0.2 mm/day through the intermountain west and southwest with drying through the north-
350 west (a decrease in mean precipitation of 0.2 mm/day). These trends largely hold and intensify
351 through the end of century (end), except in the intermountain west and southwest regions where
352 precipitation again falls to historical levels. **Statistical significance of these results is depicted in**
353 **Figure 6[Huang: Stippling is added for Pr.]**.

354 The increase in cool season precipitation in the Northwest is largely driven by increased inte-
355 grated vapor transport (IVT) (see Figure 8a). IVT is particularly useful for understanding extreme
356 precipitation events that arise from large-scale meteorological features (Ralph et al. 2004; Leung
357 and Qian 2009; Dettinger 2011). IVT is composed of absolute humidity and wind velocity, which
358 are both impacted by the climate change signal. To understand how these two factors respond
359 to the climate change signal and contribute to the increase in IVT, specific humidity and wind
360 vectors are plotted in Figure 8b. Over the eastern Pacific, we observe increases in both water
361 vapor content and wind speed, which are in turn responsible for increases to IVT in the Pacific
362 Northwest. However, over the continent we see a weakening of the westerlies overland driven
363 by a reduced meridional temperature contrast. The increased cool-season IVT does not manifest
364 strongly along the Pacific coast off of California, where IVT is much smaller on average and is
365 primarily modulated by ENSO.

366 Changes in precipitation over the Intermountain West and Southwest during the warm season are
367 primarily associated with convective processes and so are directly impacted by variations in RH.
368 As shown in Figure 5, RH increases through mid-century in this region (although with modest
369 significance) and then significantly decreases through end-of-century over most the study area
370 (except over where soil moisture was already low in hist). This results in a modest increase in
371 precipitation through mid-century followed by a return to historical precipitation amounts by end-
372 of-century. Further climate warming is expected to further decrease RH and drive increased aridity
373 in this region.

374 *b. Precipitation indices*

375 We now analyze observed changes to the precipitation indices given in Table 1. For each index,
376 the change for each period, yearly averaged over all ensemble members are plotted in Figure 6 (for

377 the indices that quantify precipitation days) and Figure 7 (for the indices describing precipitation
378 amounts).

379 On comparing `hist` and `mid`, it is clear that the number of rainy days and frequency of non-
380 extreme precipitation events (≤ 10 mm/day) have increased significantly (about 10-15%) over the
381 southwest and intermountain west, which is less obvious between `mid` and `end`. On the contrary,
382 the frequency of non-extreme precipitation have decreased significantly over the northwest region
383 and the eastern areas of the Montana, Wyoming and Oregon (by about 10%). The increase in
384 the frequency of these non-extreme precipitation events explain the observed change to mean
385 precipitation exhibited in Figure 5, and are largely associated with warm season mesoscale storm
386 systems.

387 Although essentially all regions exhibit an increase in the most extreme precipitation events (Pr
388 ≥ 10 mm/day), this increase is only statistically significant through the intermountain west and
389 in the Pacific northwest (for $Pr \geq 20$ mm/day). When comparing `mid` to `end`, there is a clear
390 and significant increase in extreme precipitation events over the northwest coast ($\sim 20\text{-}30\%$) and
391 eastern flank of the Cascades ($> 40\%$). This result is consistent with the result of Dominguez
392 et al. (2012), who observe a robust increase in winter precipitation extremes toward the latter half
393 of the 21st century with an ensemble of RCMs. The increase in the northwest is accompanied by
394 a decrease in non-extreme precipitation days, indicative of drying over the warm season.

395 [Paul: For each region it would be extremely valuable to include changes to the return frequency
396 of the most extreme events – i.e. in the Northwest a five-year storm becomes a two-year storm]

397 Notably, our results show no significant change in precipitation character is predicted for Cali-
398 fornia. In fact, the precipitation signal under a warmer climate is more ambiguous for California
399 (Neelin et al. 2013) in light of the extreme variability of the region on interannual time scales
400 (Dettinger 2011). Kim (2005) found that under global warming, heavy precipitation events in-

crease in frequency in the mountainous regions of the northern California Coastal Range and the Sierra Nevada. However, our results show a small decrease in extreme precipitation over the Sierra Nevada (although the decrease is not statistically significant). This leads us to the likely conclusion (particularly in light of VR-CESM's own biases in this region) that projections in this region are highly dependent on model formulation.

For the most extreme precipitation events ($\text{Pr} \geq 40 \text{ mm/day}$), there is a statistically significant increase along the northwest coast ($\geq 60\%$), the Cascades ($\sim 50\%$) and Northern Rockies ($\geq 60\%$) by end-of-century. Significant increases are also apparent along the Klamath range in California of about 20-40% from hist to end. Changes in accumulated precipitation for these events are consistent with the change in their frequency (see Figure 7). With a projected increase of temperatures in this region of 4-5 K over the cool season, this increase is in excess of the 7% per degree change that would be anticipated from the C-C relationship (Figure 8a). In this case, the probable cause of this excess is due to the intensification of the storm track along the coast discussed in section a.

[Paul: Check]

415 c. Regional precipitation frequency distributions

To further investigate the regional heterogeneity of changing precipitation, frequency distributions of daily rainfall for rainy days are plotted in Figure 9 for (a) the Pacific Northwest, including Washington and Oregon, (b) California, (c) the Intermountain West, including Nevada and Utah and (d) the Southwest, including Arizona and New Mexico [Paul: Region labels need to be moved earlier in the text, and we probably need a figure to identify how we refer to regions (add Northern Rockies (Idaho, Montana and Wyoming) and Great Plains (Dakotas through north Texas)). Frequency plots are developed using simulation outputs at all grid points within each region. [Paul: As discussed, need to split these plots into non-extreme / extreme] Over the Northwest, precip-

itation intensifies with upper tail going more extreme in the future, especially during end. No apparent changes can be observed for the California region, except with more extreme upper tail for Pr exceeding 100 mm/day during end, which is due to the increased precipitation extremes over the northern California as shown in Figure 7. Over the inter-mountainous region, similar trends of changes can be seen as the northwest area, with intensified mean and extreme precipitation. For the southwest area, precipitation tends to be more extreme with a moderate level, although no notable difference exists between mid and end.

d. Disentangling the direct climate signal from ENSO and PDO

As discussed earlier, this study assumes a fixed pattern of SSTs that is consistent across all ensemble members and incorporates certain assumptions on the character of ENSO through the end-of-century that arise from the coupled model. The phase of ENSO is well known to have important repercussions for precipitation extremes (Larkin and Harrison 2005; Allan and Soden 2008; Maloney et al. 2014; Yoon et al. 2015). In particular, Cai et al. (2014) found a significant increase in extraordinary precipitation events through the eastern Pacific Ocean in the 21st century within the CMIP5 ensemble, associated with increasing frequency of extreme El Niño events due to greenhouse warming. To better understand how ENSO has impacted our results, we now turn our attention to understanding how precipitation extremes behave in response to the phase of ENSO.

In our study, mean SSTs over the Niño 3.4 region are 26.83, 28.62 and 30.54°C for textsfhist, mid and end respectively. Based on the ONI index values, the mean SST anomalies are 1.38, 1.71 and 2.30 K during El Niño years, and -1.16, -1.62 and -1.43 K during La Niña years, again for hist, mid and end. It is apparent within that within this dataset the magnitude of SST anomalies associated with ENSO has intensified. SST anomalies of each year and each month, and their

447 associated spatial pattern when averaged over the warm and cool phases of ENSO can be found in
448 the supplement, suggesting an increasing frequency of El Niño through mid and an almost doubled
449 frequency of La Niña during mid and end compared to the hist.

450 [Huang: As SSTs increase in the future, is not it normal for the anomaly of ENSO to be increased
451 to compensate the changes of water vapor capacity? Might email Neale about this]

452 Differences in mean precipitation and associated indices taken between the warm phase (i.e.
453 El Niño) and cool phase (i.e. La Niña) of ENSO are provided in Figure 10 for the cool seasons
454 from hist, mid and end. During the El Niño phase, intensified mean precipitation is expected
455 over California and the southwest (Hamlet and Lettenmaier 2007), accompanied by reduced pre-
456 cipitation intensity over the northwest. In the La Niña phase, this pattern is reversed, with wetter
457 conditions in the northwest and a drier southwest. Consequently, ENSO is associated with a
458 northwest/southwest precipitation dipole, triggered by ENSO's modification of the storm track
459 (Gershunov and Barnett 1998; Leung et al. 2003b), along with modulation of the enhanced pre-
460 cipitation variability (Cayan et al. 1999; Kahya and Dracup 1994). Strengthening storm patterns
461 associated with ENSO are also found by Maloney et al. (2014) over California using CMIP5
462 output under RCP8.5. This dipole is also apparent in the frequency of rainy days and extreme
463 precipitation events.

464 The impact of ENSO can also be seen in the IVT difference that arises between El Niño and
465 La Niña phases in each time period (see Figure 11) and the accompanying 850 hPa wind patterns.
466 During the El Niño phase, there is an increase in on-shore moisture flux over California that
467 triggers a returning circulation through the northwest. This suggests that understanding moisture
468 flux regulation from ENSO is a very important contributor to the character of future precipitation
469 extremes.

470 Based on the above results, it is apparent that the magnitude of the effects of ENSO is compa-
471 rable or even higher than the impacts of climate forcing – that is, shifts in the future character of
472 ENSO would have more dire implications for precipitation extremes than shifts in mean climato-
473 logical forcing. To investigate this further, linear regression has applied at each grid point using
474 a simple linear model that incorporates the phase of ENSO (using the Niño 3.4 SST anomaly)
475 and the underlying climate forcing (from mean GHG concentration). The precipitation indices are
476 used as response variables. The significance of these two factors was then obtained from ANOVA
477 (analysis of variance) output (see the supplement [\[Paul: Point to lm_fit_pvalue\]](#)). The magnitude
478 of the response associated with each factor was also computed (see the supplement [\[Paul: Point](#)
479 [to wd_lmfit_coef_enso_ghg\]](#)). As expected, the ENSO forcing matches most closely with the dif-
480 ference between El Niño and La Niña (see Figure 11). Hence, we observe that ENSO is a major
481 driver of precipitation character through California, the intermountain west and the southwest and
482 does have an impact on mean precipitation through the Cascades. In contrast, the impacts of cli-
483 mate forcing are visually similar to the pattern of the difference between the different time periods
484 (see Figure 6), and primarily impacts both extreme and non-extreme precipitation in the northwest
485 and intermountain west.

486 We have also assessed the impacts of the Pacific Decadal Oscillation (PDO) on precipitation and
487 observed only a weak correlation between the PDO pattern and precipitation. That is, precipita-
488 tion features did not change substantially between the cool phase or warm phase of PDO when
489 examining hist data. However, when in phase with ENSO, PDO did have a notable impact over
490 the northwest. This coupled effect has been found by previous studies Gershunov and Barnett
491 (1998), who observed that ENSO and PDO can “reinforce” each other, with PDO responding to
492 the same internal atmospheric variability as ENSO (Pierce 2002). In our simulations, there were
493 roughly an equal number of positive PDO years and negative PDO years in the data from each

494 time period, but since SSTs were fixed among ensemble members, the 26 year simulation period
495 might be insufficient to account for the variability of PDO. Therefore, in this study we draw no
496 conclusions on the impact of PDO.

497 **7. Discussion and Summary**

498 The increased cool season precipitation extremes tend to result in higher runoff events over
499 the northwest U.S., which are in turn associated with a greater chance of flooding and a loss of
500 snowpack. A decrease in counts of rainy days during the warm season over central and southern
501 California, though small in magnitude, will probably intensify the drought condition due to the
502 deficit of soil moisture with higher evapotranspiration caused by the warmer climate in the future
503 Cayan et al. (2010); Bell et al. (2004).

504 (Summary is to be added once the main content have been settled down The contribution of
505 human-induced increases in greenhouse gases to the character of precipitation is confounded by
506 patterns of variability in the atmospheric circulation. Consistent with previous studies, changes
507 in more extreme precipitation follow the Clausius-Clapeyron relationship more closely than total
508 precipitation amount. The changes of the strength of ENSO remains uncertain. However, the char-
509 acter of ENSO appears to be the largest factor in understanding changing precipitation extremes
510 in the U.S. West.)

511 Notes for the summary:

- 512 • Northwest: Increase in extreme precipitation events (state return time of 20mm/day and
513 40mm/day events) accompanied by a substantial moistening of the cool season, even though
514 total precipitation days doesn't change. This is driven by increased IVT over the eastern
515 Pacific. Increased drying over the warm season driven by a reduction in RH.

- 516 • California: No clear climate signal in mean precipitation or extremes. Precipitation in this
517 area is dominated by interannual variability, primarily associated with ENSO.
- 518 • Intermountain West and Southwest: Increase in warm season RH through mid-century fol-
519 lowed by a reduced RH through end-of-century. Nonetheless accompanied by a statistically
520 significant increase in Pr and non-extreme rainy days due to increased convection (?)

521 *Acknowledgments.* The authors would like to thank Michael Wehner for sharing the dataset and
522 many suggestions. The authors also want to thank Alan M. Rhoades for providing the simulation
523 output. We acknowledge the substantial efforts behind the datasets used in this study, including
524 UW, NCDC and NARR. The simulation data used is available by request at xyhuang@ucdavis.edu.
525 This project is supported in part by the xxx and by the xxx.

526 References

- 527 AchutaRao, K., and K. R. Sperber, 2006: Enso simulation in coupled ocean-atmosphere models:
528 are the current models better? *Climate Dynamics*, **27** (1), 1–15.
- 529 Allan, R. P., and B. J. Soden, 2008: Atmospheric warming and the amplification of precipitation
530 extremes. *Science*, **321** (5895), 1481–1484.
- 531 Allen, M. R., and W. J. Ingram, 2002: Constraints on future changes in climate and the hydrologic
532 cycle. *Nature*, **419** (6903), 224–232.
- 533 Bell, J. L., L. C. Sloan, and M. A. Snyder, 2004: Regional changes in extreme climatic events: a
534 future climate scenario. *Journal of Climate*, **17** (1), 81–87.
- 535 Cai, W., and Coauthors, 2014: Increasing frequency of extreme el niño events due to greenhouse
536 warming. *Nature climate change*, **4** (2), 111–116.

- 537 Caldwell, P., 2010: California wintertime precipitation bias in regional and global climate models.
- 538 *Journal of Applied Meteorology and Climatology*, **49** (10), 2147–2158.
- 539 Capotondi, A., 2013: Enso diversity in the ncar ccm4 climate model. *Journal of Geophysical*
- 540 *Research: Oceans*, **118** (10), 4755–4770.
- 541 Cayan, D. R., T. Das, D. W. Pierce, T. P. Barnett, M. Tyree, and A. Gershunov, 2010: Future
- 542 dryness in the southwest us and the hydrology of the early 21st century drought. *Proceedings of*
- 543 *the National Academy of Sciences*, **107** (50), 21 271–21 276.
- 544 Cayan, D. R., K. T. Redmond, and L. G. Riddle, 1999: ENSO and hydrologic extremes in the
- 545 western United States*. *Journal of Climate*, **12** (9), 2881–2893.
- 546 Collins, M., and Coauthors, 2010: The impact of global warming on the tropical pacific ocean and
- 547 el niño. *Nature Geoscience*, **3** (6), 391–397.
- 548 Dennis, J., and Coauthors, 2011: CAM-SE: A scalable spectral element dynamical core for the
- 549 Community Atmosphere Model. *International Journal of High Performance Computing Appli-*
- 550 *cations*, 1094342011428142.
- 551 Deser, C., R. Knutti, S. Solomon, and A. S. Phillips, 2012a: Communication of the role of natural
- 552 variability in future north american climate. *Nature Climate Change*, **2** (11), 775–779.
- 553 Deser, C., A. Phillips, V. Bourdette, and H. Teng, 2012b: Uncertainty in climate change projec-
- 554 tions: the role of internal variability. *Climate Dynamics*, **38** (3-4), 527–546.
- 555 Deser, C., and Coauthors, 2012c: Enso and pacific decadal variability in the community climate
- 556 system model version 4. *Journal of Climate*, **25** (8), 2622–2651.
- 557 Dettinger, M., 2011: Climate change, atmospheric rivers, and floods in california—a multimodel
- 558 analysis of storm frequency and magnitude changes1. Wiley Online Library.

- 559 Diffenbaugh, N. S., J. S. Pal, R. J. Trapp, and F. Giorgi, 2005: Fine-scale processes regulate the
560 response of extreme events to global climate change. *Proceedings of the National Academy of*
561 *Sciences of the United States of America*, **102** (44), 15 774–15 778.
- 562 DiNezio, P. N., B. P. Kirtman, A. C. Clement, S.-K. Lee, G. A. Vecchi, and A. Wittenberg, 2012:
563 Mean climate controls on the simulated response of enso to increasing greenhouse gases. *Journal*
564 *of Climate*, **25** (21), 7399–7420.
- 565 Dominguez, F., E. Rivera, D. Lettenmaier, and C. Castro, 2012: Changes in winter precipitation
566 extremes for the western united states under a warmer climate as simulated by regional climate
567 models. *Geophysical Research Letters*, **39** (5).
- 568 Donat, M. G., A. L. Lowry, L. V. Alexander, P. A. OGorman, and N. Maher, 2016: More extreme
569 precipitation in the world's dry and wet regions. *Nature Climate Change*.
- 570 Duffy, P., and Coauthors, 2006: Simulations of present and future climates in the western United
571 States with four nested regional climate models. *Journal of Climate*, **19** (6), 873–895.
- 572 Duli  re, V., Y. Zhang, and E. P. Salath   Jr, 2011: Extreme Precipitation and Temperature over the
573 US Pacific Northwest: A Comparison between Observations, Reanalysis Data, and Regional
574 Models*. *Journal of Climate*, **24** (7), 1950–1964.
- 575 Easterling, D. R., G. A. Meehl, C. Parmesan, S. A. Changnon, T. R. Karl, and L. O. Mearns, 2000:
576 Climate extremes: observations, modeling, and impacts. *science*, **289** (5487), 2068–2074.
- 577 Fedorov, A. V., and S. G. Philander, 2000: Is el ni  o changing? *Science*, **288** (5473), 1997–2002.
- 578 Fox-Rabinovitz, M., J. C  te, B. Dugas, M. D  qu  , and J. L. McGregor, 2006: Variable resolution
579 general circulation models: Stretched-grid model intercomparison project (SGMIP). *Journal of*
580 *Geophysical Research: Atmospheres (1984–2012)*, **111** (D16).

- 581 Fox-Rabinovitz, M. S., G. L. Stenchikov, M. J. Suarez, and L. L. Takacs, 1997: A finite-
582 difference GCM dynamical core with a variable-resolution stretched grid. *Monthly weather*
583 *review*, **125** (11), 2943–2968.
- 584 Frei, C., R. Schöll, S. Fukutome, J. Schmidli, and P. L. Vidale, 2006: Future change of precipita-
585 tion extremes in Europe: Intercomparison of scenarios from regional climate models. *Journal*
586 *of Geophysical Research: Atmospheres (1984–2012)*, **111** (D6).
- 587 Gao, Y., J. Lu, L. R. Leung, Q. Yang, S. Hagos, and Y. Qian, 2015: Dynamical and thermodynami-
588 cal modulations on future changes of landfalling atmospheric rivers over western north america.
589 *Geophysical Research Letters*, **42** (17), 7179–7186.
- 590 Gates, W. L., 1992: AMIP: The Atmospheric Model Intercomparison Project. *Bulletin of the*
591 *American Meteorological Society*, **73**, 1962–1970.
- 592 Gershunov, A., and T. P. Barnett, 1998: Interdecadal modulation of enso teleconnections. *Bulletin*
593 *of the American Meteorological Society*, **79** (12), 2715–2725.
- 594 Gettelman, A., H. Morrison, and S. J. Ghan, 2008: A new two-moment bulk stratiform cloud
595 microphysics scheme in the Community Atmosphere Model, version 3 (CAM3). Part II: Single-
596 column and global results. *Journal of Climate*, **21** (15), 3660–3679.
- 597 Grodsky, S. A., J. A. Carton, S. Nigam, and Y. M. Okumura, 2012: Tropical atlantic biases in
598 ccsm4. *Journal of Climate*, **25** (11), 3684–3701.
- 599 Guilyardi, E., A. Wittenberg, A. Fedorov, M. Collins, C. Wang, A. Capotondi, G. J. Van Olden-
600 borg, and T. Stockdale, 2009: Understanding el niño in ocean-atmosphere general circulation
601 models. *Bulletin of the American Meteorological Society*, **90** (3), 325.

- 602 Hamlet, A. F., and D. P. Lettenmaier, 2005: Production of Temporally Consistent Gridded Precipi-
603 tation and Temperature Fields for the Continental United States*. *Journal of Hydrometeorology*,
604 **6** (3), 330–336.
- 605 Hamlet, A. F., and D. P. Lettenmaier, 2007: Effects of 20th century warming and climate variability
606 on flood risk in the western us. *Water Resources Research*, **43** (6).
- 607 Hegerl, G. C., F. W. Zwiers, P. A. Stott, and V. V. Kharin, 2004: Detectability of anthropogenic
608 changes in annual temperature and precipitation extremes. *Journal of Climate*, **17** (19), 3683–
609 3700.
- 610 Huang, X., A. M. Rhoades, P. A. Ullrich, and C. M. Zarzycki, 2016: An evaluation of the vari-
611 able resolution-cesm for modeling california’s climate. *Journal of Advances in Modeling Earth
612 Systems*.
- 613 Huang, X., and P. A. Ullrich, 2016: Irrigation impacts on california’s climate with the variable-
614 resolution cesm. *Journal of Advances in Modeling Earth Systems*.
- 615 Hurrell, J. W., J. J. Hack, D. Shea, J. M. Caron, and J. Rosinski, 2008: A new sea surface temper-
616 ature and sea ice boundary dataset for the Community Atmosphere Model. *Journal of Climate*,
617 **21** (19), 5145–5153.
- 618 Hurrell, J. W., and Coauthors, 2013: The community earth system model: A framework for col-
619 laborative research. *Bulletin of the American Meteorological Society*, **94** (9), 1339–1360.
- 620 Jha, B., Z.-Z. Hu, and A. Kumar, 2014: Sst and enso variability and change simulated in historical
621 experiments of cmip5 models. *Climate dynamics*, **42** (7-8), 2113–2124.
- 622 Joseph, R., and S. Nigam, 2006: Enso evolution and teleconnections in ipcc’s twentieth-century
623 climate simulations: Realistic representation? *Journal of Climate*, **19** (17), 4360–4377.

- 624 Joshi, M. M., J. M. Gregory, M. J. Webb, D. M. Sexton, and T. C. Johns, 2008: Mechanisms for
625 the land/sea warming contrast exhibited by simulations of climate change. *Climate Dynamics*,
626 **30** (5), 455–465.
- 627 Kahya, E., and J. A. Dracup, 1994: The influences of type 1 el nino and la nina events on stream-
628 flows in the pacific southwest of the united states. *Journal of Climate*, **7** (6), 965–976.
- 629 Kao, H.-Y., and J.-Y. Yu, 2009: Contrasting eastern-pacific and central-pacific types of enso.
630 *Journal of Climate*, **22** (3), 615–632.
- 631 Karl, T. R., N. Nicholls, and A. Ghazi, 1999: Clivar/gcos/wmo workshop on indices and indicators
632 for climate extremes workshop summary. *Weather and Climate Extremes*, Springer, 3–7.
- 633 Kharin, V. V., F. W. Zwiers, X. Zhang, and G. C. Hegerl, 2007: Changes in temperature and
634 precipitation extremes in the IPCC ensemble of global coupled model simulations. *Journal of*
635 *Climate*, **20** (8), 1419–1444.
- 636 Kim, J., 2005: A projection of the effects of the climate change induced by increased co2 on
637 extreme hydrologic events in the western us. *Climatic Change*, **68** (1-2), 153–168.
- 638 Laprise, R., and Coauthors, 2008: Challenging some tenets of regional climate modelling. *Meteo-*
639 *rology and Atmospheric Physics*, **100** (1-4), 3–22.
- 640 Larkin, N. K., and D. Harrison, 2005: On the definition of el niño and associated seasonal average
641 us weather anomalies. *Geophysical Research Letters*, **32** (13).
- 642 Latif, M., and N. S. Keenlyside, 2009: El niño/southern oscillation response to global warming.
643 *Proceedings of the National Academy of Sciences*, **106** (49), 20 578–20 583.
- 644 Leung, L. R., L. O. Mearns, F. Giorgi, and R. L. Wilby, 2003a: Regional climate research: needs
645 and opportunities. *Bulletin of the American Meteorological Society*, **84** (1), 89–95.

- 646 Leung, L. R., and Y. Qian, 2009: Atmospheric rivers induced heavy precipitation and flooding in
647 the western US simulated by the WRF regional climate model. *Geophysical research letters*,
648 **36** (3).
- 649 Leung, L. R., Y. Qian, and X. Bian, 2003b: Hydroclimate of the western United States based on
650 observations and regional climate simulation of 1981-2000. Part I: Seasonal statistics. *Journal*
651 *of Climate*, **16** (12), 1892–1911.
- 652 Maloney, E. D., and Coauthors, 2014: North american climate in cmip5 experiments: part iii:
653 assessment of twenty-first-century projections*. *Journal of Climate*, **27** (6), 2230–2270.
- 654 Maurer, E., A. Wood, J. Adam, D. Lettenmaier, and B. Nijssen, 2002: A long-term hydrologically
655 based dataset of land surface fluxes and states for the conterminous United States*. *Journal of*
656 *climate*, **15** (22), 3237–3251.
- 657 McDonald, A., 2003: Transparent boundary conditions for the shallow-water equations: testing in
658 a nested environment. *Monthly weather review*, **131** (4), 698–705.
- 659 Meehl, G. A., H. Teng, and G. Bannister, 2006: Future changes of el niño in two global coupled
660 climate models. *Climate Dynamics*, **26** (6), 549–566.
- 661 Mesinger, F., and K. Veljovic, 2013: Limited area NWP and regional climate modeling: a test
662 of the relaxation vs Eta lateral boundary conditions. *Meteorology and Atmospheric Physics*,
663 **119** (1-2), 1–16.
- 664 Mesinger, F., and Coauthors, 2006: North American regional reanalysis. *Bulletin of the American*
665 *Meteorological Society*, **87**, 343–360.
- 666 Min, S.-K., X. Zhang, F. W. Zwiers, and G. C. Hegerl, 2011: Human contribution to more-intense
667 precipitation extremes. *Nature*, **470** (7334), 378–381.

668 Morrison, H., and A. Gettelman, 2008: A new two-moment bulk stratiform cloud microphysics
669 scheme in the Community Atmosphere Model, version 3 (CAM3). Part I: Description and nu-
670 numerical tests. *Journal of Climate*, **21** (15), 3642–3659.

671 Neale, R. B., and Coauthors, 2010a: Description of the NCAR community atmosphere model
672 (CAM 5.0). *NCAR Tech. Note NCAR/TN-486+STR*.

673 Neale, R. B., and Coauthors, 2010b: Description of the NCAR Community Atmosphere Model
674 (CAM 5.0). NCAR Technical Note NCAR/TN-486+STR, National Center for Atmospheric Re-
675 search, Boulder, Colorado, 268 pp.

676 Neelin, J. D., B. Langenbrunner, J. E. Meyerson, A. Hall, and N. Berg, 2013: California winter
677 precipitation change under global warming in the coupled model intercomparison project phase
678 5 ensemble. *Journal of Climate*, **26** (17), 6238–6256.

679 Neiman, P. J., F. M. Ralph, G. A. Wick, J. D. Lundquist, and M. D. Dettinger, 2008: Meteorolog-
680 ical characteristics and overland precipitation impacts of atmospheric rivers affecting the west
681 coast of north america based on eight years of ssm/i satellite observations. *Journal of Hydrom-
682 eteorology*, **9** (1), 22–47.

683 NOAA, 2013: Defining El Niño and La Niña. Accessed: 2015-
684 08-20, [https://www.climate.gov/news-features/understanding-climate/
685 watching-el-nio-and-la-nia-noaa-adapts-global-warming](https://www.climate.gov/news-features/understanding-climate/watching-el-nio-and-la-nia-noaa-adapts-global-warming).

686 O’Gorman, P. A., and T. Schneider, 2009: The physical basis for increases in precipitation ex-
687 tremes in simulations of 21st-century climate change. *Proceedings of the National Academy of
688 Sciences*, **106** (35), 14 773–14 777.

- 689 Oleson, K., and Coauthors, 2010: Technical description of version 4.0 of the Community Land
690 Model (CLM). NCAR Technical Note NCAR/TN-478+STR, National Center for Atmospheric
691 Research, Boulder, Colorado, 257 pp. doi:10.5065/D6FB50WZ.
- 692 Pierce, D. W., 2002: The role of sea surface temperatures in interactions between enso and the
693 north pacific oscillation. *Journal of climate*, **15** (11), 1295–1308.
- 694 Ralph, F. M., P. J. Neiman, and G. A. Wick, 2004: Satellite and caljet aircraft observations of
695 atmospheric rivers over the eastern north pacific ocean during the winter of 1997/98. *Monthly*
696 *Weather Review*, **132** (7), 1721–1745.
- 697 Rauscher, S. A., E. Coppola, C. Piani, and F. Giorgi, 2010: Resolution effects on regional climate
698 model simulations of seasonal precipitation over Europe. *Climate dynamics*, **35** (4), 685–711.
- 699 Rauscher, S. A., T. D. Ringler, W. C. Skamarock, and A. A. Mirin, 2013: Exploring a Global
700 Multiresolution Modeling Approach Using Aquaplanet Simulations. *Journal of Climate*, **26** (8),
701 2432–2452.
- 702 Rhoades, A. M., X. Huang, P. A. Ullrich, and C. M. Zarzycki, 2015: Characterizing Sierra Nevada
703 snowpack using variable-resolution CESM. *Journal of Applied Meteorology and Climatology*,
704 (2015).
- 705 Riahi, K., and Coauthors, 2011: RCP 8.5A scenario of comparatively high greenhouse gas emis-
706 sions. *Climatic Change*, **109** (1-2), 33–57.
- 707 Rowell, D. P., and R. G. Jones, 2006: Causes and uncertainty of future summer drying over europe.
708 *Climate Dynamics*, **27** (2-3), 281–299.

- 709 Salathé Jr, E. P., R. Steed, C. F. Mass, and P. H. Zahn, 2008: A High-Resolution Climate Model
710 for the US Pacific Northwest: Mesoscale Feedbacks and Local Responses to Climate Change*.
711 *Journal of Climate*, **21** (21), 5708–5726.
- 712 Scoccimarro, E., M. Zampieri, A. Bellucci, A. Navarra, and Coauthors, 2013: Heavy precipitation
713 events in a warmer climate: results from CMIP5 models. *Journal of climate*.
- 714 Seneviratne, S. I., and Coauthors, 2012: Changes in climate extremes and their impacts on the
715 natural physical environment. *Managing the risks of extreme events and disasters to advance*
716 *climate change adaptation*, 109–230.
- 717 Sillmann, J., V. Kharin, F. Zwiers, X. Zhang, and D. Bronaugh, 2013: Climate extremes indices
718 in the cmip5 multimodel ensemble: Part 2. future climate projections. *Journal of Geophysical*
719 *Research: Atmospheres*, **118** (6), 2473–2493.
- 720 Simmons, A., K. Willett, P. Jones, P. Thorne, and D. Dee, 2010: Low-frequency variations
721 in surface atmospheric humidity, temperature, and precipitation: Inferences from reanalyses
722 and monthly gridded observational data sets. *Journal of Geophysical Research: Atmospheres*,
723 **115** (D1).
- 724 Singh, D., M. Tsiang, B. Rajaratnam, and N. S. Diffenbaugh, 2013: Precipitation extremes over the
725 continental United States in a transient, high-resolution, ensemble climate model experiment.
726 *Journal of Geophysical Research: Atmospheres*, **118** (13), 7063–7086.
- 727 Small, R. J., and Coauthors, 2014: A new synoptic scale resolving global climate simulation using
728 the community earth system model. *Journal of Advances in Modeling Earth Systems*, **6** (4),
729 1065–1094.

- 730 Staniforth, A. N., and H. L. Mitchell, 1978: A variable-resolution finite-element technique for
731 regional forecasting with the primitive equations. *Monthly Weather Review*, **106** (4), 439–447.
- 732 Stevenson, S., 2012: Significant changes to enso strength and impacts in the twenty-first century:
733 Results from cmip5. *Geophysical Research Letters*, **39** (17).
- 734 Sugi, M., and J. Yoshimura, 2004: A mechanism of tropical precipitation change due to co2
735 increase. *Journal of climate*, **17** (1), 238–243.
- 736 Taschetto, A. S., A. S. Gupta, N. C. Jourdain, A. Santoso, C. C. Ummenhofer, and M. H. England,
737 2014: Cold tongue and warm pool enso events in cmip5: mean state and future projections.
738 *Journal of Climate*, **27** (8), 2861–2885.
- 739 Taylor, M. A., 2011: Conservation of mass and energy for the moist atmospheric primitive equa-
740 tions on unstructured grids. *Numerical Techniques for Global Atmospheric Models*, Springer,
741 357–380.
- 742 Tebaldi, C., K. Hayhoe, J. M. Arblaster, and G. A. Meehl, 2006: Going to the extremes. *Climatic
743 change*, **79** (3-4), 185–211.
- 744 Trenberth, K. E., 2011: Changes in precipitation with climate change. *Climate Research*, **47** (1),
745 123.
- 746 Trenberth, K. E., A. Dai, R. M. Rasmussen, and D. B. Parsons, 2003: The changing character of
747 precipitation. *Bulletin of the American Meteorological Society*, **84** (9), 1205–1217.
- 748 Ullrich, P. A., D. Devendran, and H. Johansen, 2016: Arbitrary-order conservative and consistent
749 remapping and a theory of linear maps, part 2. *Monthly Weather Review*, **144** (4), 1529–1549,
750 doi:10.1175/MWR-D-15-0301.1.

- 751 Ullrich, P. A., and M. A. Taylor, 2015: Arbitrary-Order Conservative and Consistent Remapping
752 and a Theory of Linear Maps: Part I. *Monthly Weather Review*, **143** (6), 2419–2440, doi:10.
753 1175/MWR-D-14-00343.1.
- 754 Walker, M. D., and N. S. Diffenbaugh, 2009: Evaluation of high-resolution simulations of daily-
755 scale temperature and precipitation over the united states. *Climate dynamics*, **33** (7-8), 1131–
756 1147.
- 757 Wehner, M. F., 2013: Very extreme seasonal precipitation in the NARCCAP ensemble: model
758 performance and projections. *Climate Dynamics*, **40** (1-2), 59–80.
- 759 Wehner, M. F., R. L. Smith, G. Bala, and P. Duffy, 2010: The effect of horizontal resolution
760 on simulation of very extreme US precipitation events in a global atmosphere model. *Climate
761 dynamics*, **34** (2-3), 241–247.
- 762 Wehner, M. F., and Coauthors, 2014: The effect of horizontal resolution on simulation qual-
763 ity in the Community Atmospheric Model, CAM5.1. *J. Model. Earth. Sys.*, doi:10.1002/
764 2013MS000276.
- 765 Yoon, J.-H., S. S. Wang, R. R. Gillies, B. Kravitz, L. Hipps, and P. J. Rasch, 2015: Increasing
766 water cycle extremes in california and in relation to enso cycle under global warming. *Nature
767 communications*, **6**.
- 768 Zarzycki, C. M., C. Jablonowski, and M. A. Taylor, 2014: Using Variable-Resolution Meshes
769 to Model Tropical Cyclones in the Community Atmosphere Model. *Monthly Weather Review*,
770 **142** (3), 1221–1239.

- 771 Zarzycki, C. M., C. Jablonowski, D. R. Thatcher, and M. A. Taylor, 2015: Effects of localized grid
772 refinement on the general circulation and climatology in the Community Atmosphere Model.
773 *Journal of Climate*, (2015).
- 774 Zhang, X., L. Alexander, G. C. Hegerl, P. Jones, A. K. Tank, T. C. Peterson, B. Trewin, and
775 F. W. Zwiers, 2011: Indices for monitoring changes in extremes based on daily temperature and
776 precipitation data. *Wiley Interdisciplinary Reviews: Climate Change*, **2** (6), 851–870.
- 777 Zhang, X., J. Wang, F. W. Zwiers, and P. Y. Groisman, 2010: The influence of large-scale climate
778 variability on winter maximum daily precipitation over North America. *Journal of Climate*,
779 **23** (11), 2902–2915.

780 update the mesh grid plot

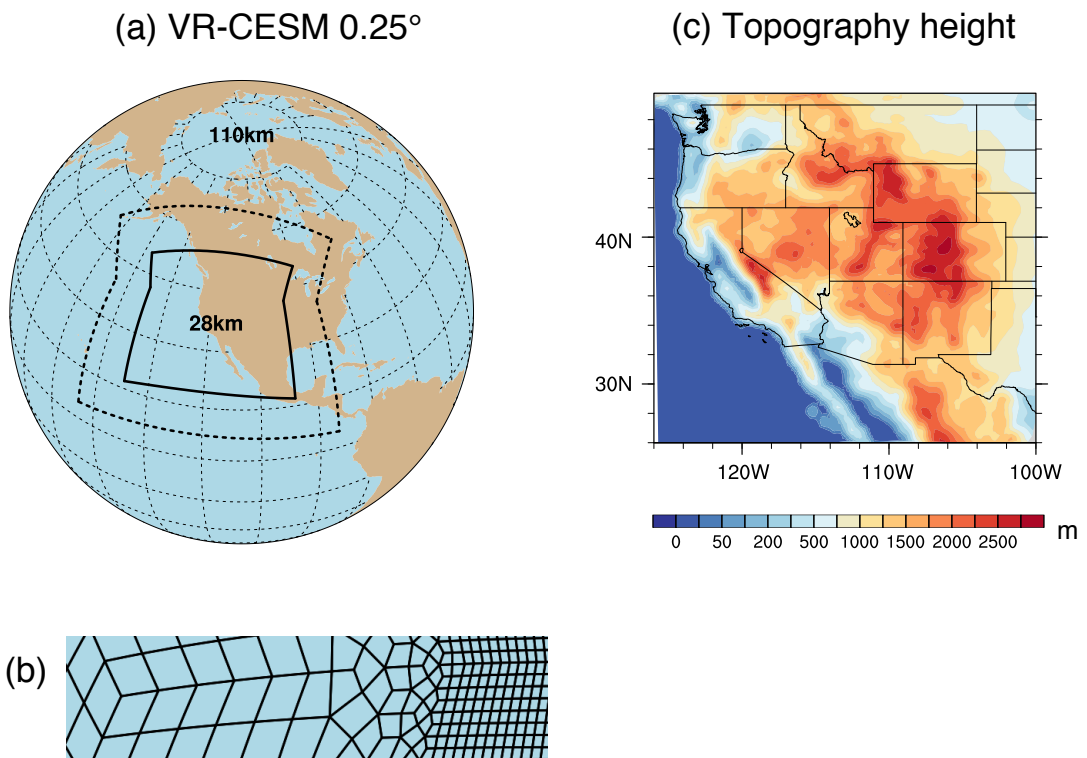
781 LIST OF TABLES

TABLE 1. Precipitation indices employed in this study.

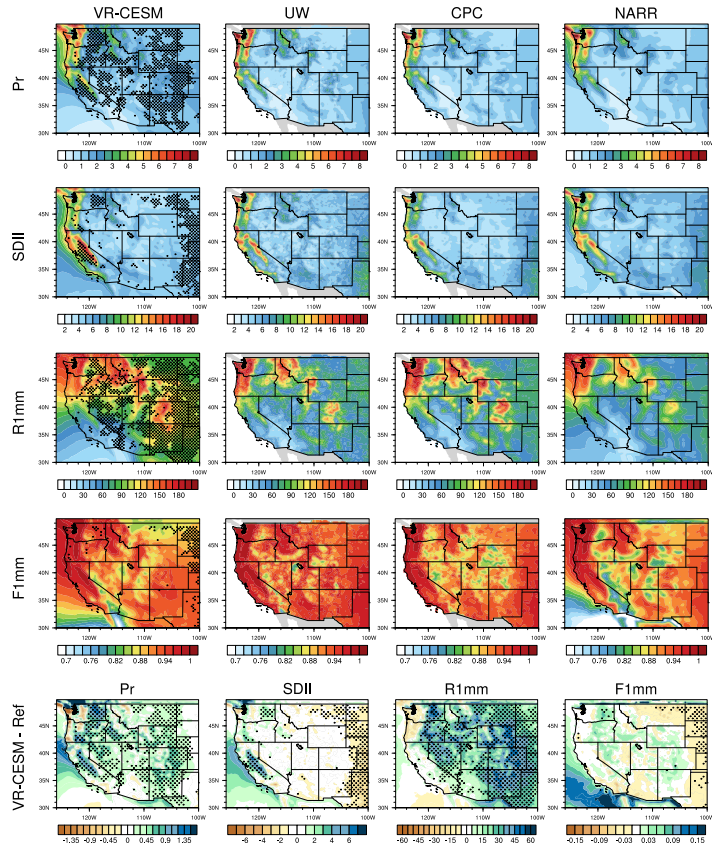
Name	Definition
Pr	Mean daily precipitation
R1mm	Number of days per year with Pr>1 mm
SDII	Simple precipitation intensity index: Precipitation amount / $\langle R1mm \rangle$ (mm/day)
R5mm	Number of days per year with Pr>1 mm and Pr=<5 mm
R10mm	Number of days per year with Pr>5 mm and Pr=<10 mm
R20mm	Number of days per year with Pr>10 mm and Pr=<20 mm
R40mm	Number of days per year with Pr>20 mm and Pr=<40 mm
Rxmm	Number of days per year with Pr>40 mm
F1mm	Fraction of precipitation contributed to the total precipitation for days of R1mm (similarly for F5mm, F10mm, F20mm, F40mm and Fxmm)
P5mm	Precipitation amount from R5mm (similarly for P10mm, P20mm, F40mm, Pxmm)

783 **LIST OF FIGURES**

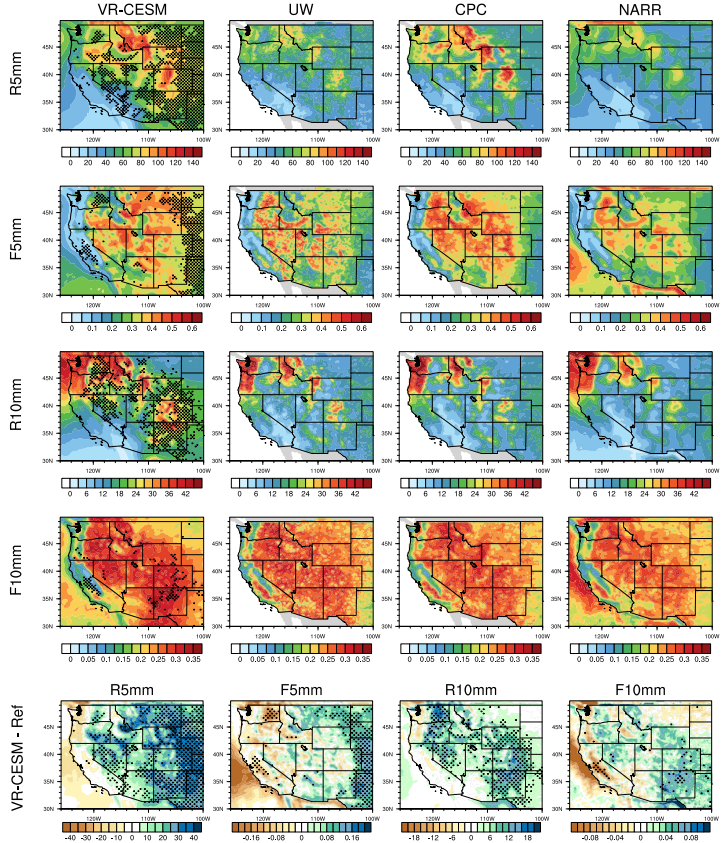
784 Fig. 1.	(a) The approximate grid spacing used for the VR-CESM 0.25° mesh. (b) A depiction of 785 the transition from the global 1° resolution mesh through two layers of refinement to 0.25° . 786 (c) Topography height over the study area.	41
787 Fig. 2.	Mean precipitation and other related indices from VR-CESM and reference datasets over 788 1980-2005. (Note: Grids with statistically significance difference between VR-CESM and 789 references mean are marked with stippling.)	42
790 Fig. 3.	The mean precipitation and other related indices from VR-CESM and reference datasets 791 over 1980-2005 (continued).	43
792 Fig. 4.	The mean precipitation and other related indices from VR-CESM and reference datasets 793 over 1980-2005 (continued).	44
794 Fig. 5.	The mean precipitation (Pr), 2m average temperature ($Tavg$), and 2m relative humidity (RH) 795 averaged over each time period. (Note: Grids with statistically significance difference for 796 the RH and Pr are marked with stippling)	45
797 Fig. 6.	Differences of precipitation behaviors from past to future over WUS averaged of each time 798 period. (Note: Grids with statistically significance difference are marked with stippling)	46
799 Fig. 7.	Differences of precipitation behaviors from past to future over WUS averaged of each time 800 period (continued).	47
801 Fig. 8.	Changes of specific humidity and horizontal wind pattern at 850hPa for moisture flux il- 802 lustration, and IVT for simulations under different time period of wet season (October to 803 March) averaged over 26 years. (Note: The minimum wind vector is set to be 0.5 m/s, 804 therefore, the wind less than 0.5 m/s is also plotted at the minimum length for better vis- 805 ualization.) Specific humidity and wind pattern are averaged over all days over cool season 806 rather than days with $Pr \geq 10\text{mm}$.	48
807 Fig. 9.	Frequency distribution of rainy days ($Pr \geq 0.1\text{mm/day}$) over the three time periods from 808 simulations in four regions (with logarithmic vertical scale). (Note: Region 1 to 4 cover 809 Washington and Oregon; California; Nevada, Utah and Idaho; Arizona and New Mexico, 810 respectively)	49
811 Fig. 10.	Difference of precipitation behaviors between warm and cool phases of ENSO from past to 812 future over WUS averaged of each time period.	50
813 Fig. 11.	Changes of IVT for simulations under different phases of ENSO of wet season (October to 814 March). (Note: The minimum wind vector is set to be 0.5 m/s, therefore, the wind less than 815 0.5 m/s is also plotted at the minimum length for better visualization.)	51



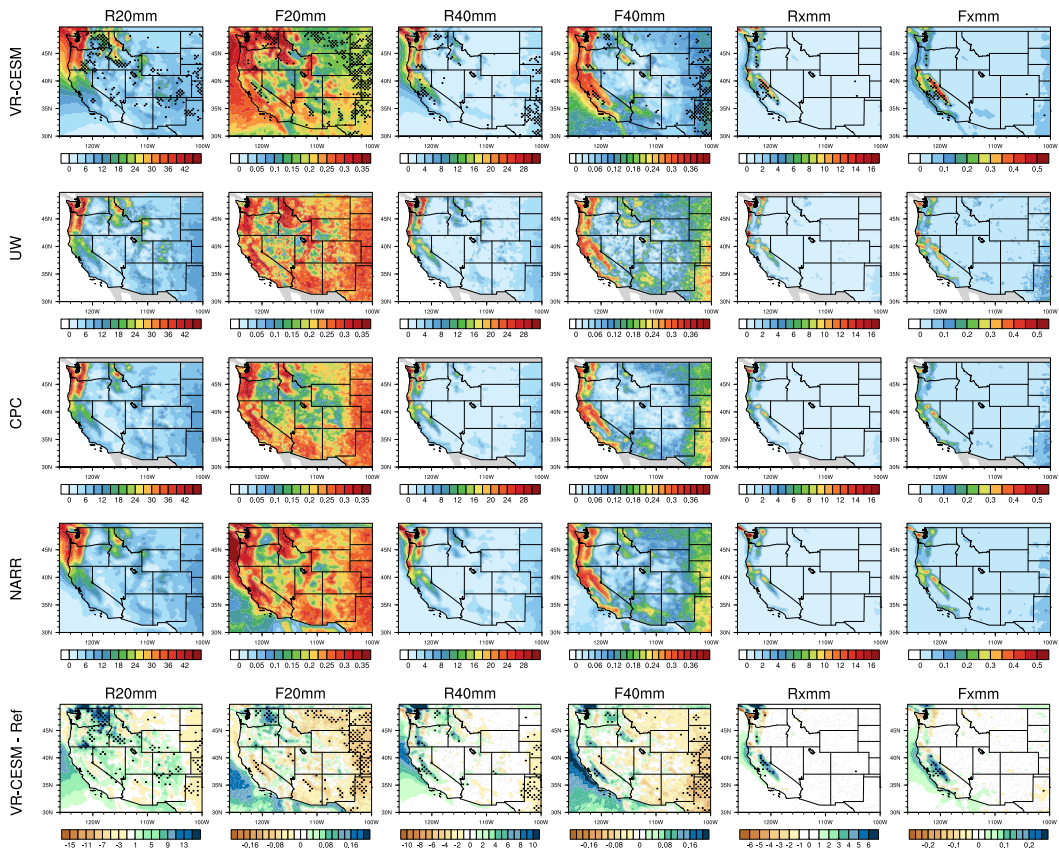
816 FIG. 1. (a) The approximate grid spacing used for the VR-CESM 0.25° mesh. (b) A depiction of the transition
 817 from the global 1° resolution mesh through two layers of refinement to 0.25° . (c) Topography height over the
 818 study area.



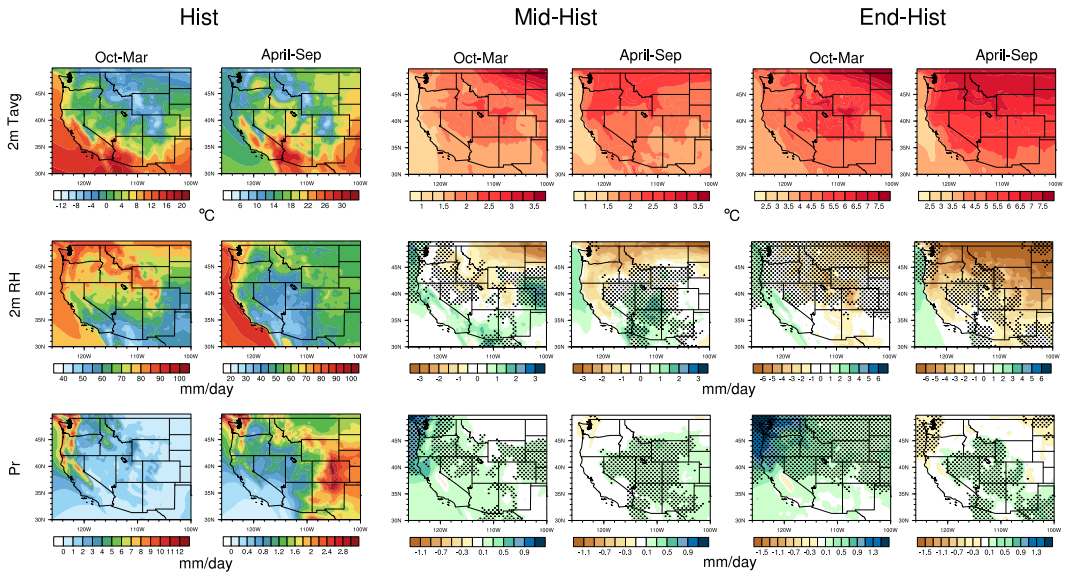
819 FIG. 2. Mean precipitation and other related indices from VR-CESM and reference datasets over 1980-2005.
820 (Note: Grids with statistically significant difference between VR-CESM and references mean are marked with
821 stippling.)



822 FIG. 3. The mean precipitation and other related indices from VR-CESM and reference datasets over 1980-
823 2005 (continued).



824 FIG. 4. The mean precipitation and other related indices from VR-CESM and reference datasets over 1980-
825 2005 (continued).



826 FIG. 5. The mean precipitation (Pr), 2m average temperature (Tavg), and 2m relative humidity (RH) averaged
 827 over each time period. (Note: Grids with statistically significant difference for the RH and Pr are marked with
 828 stippling.)

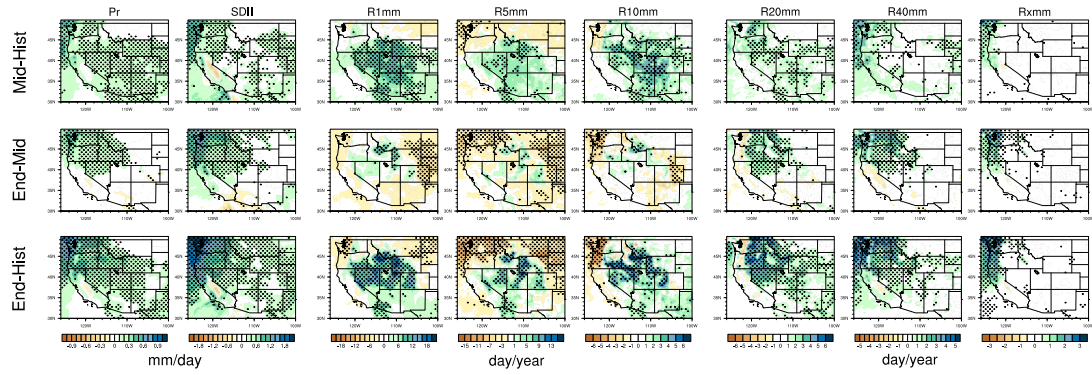
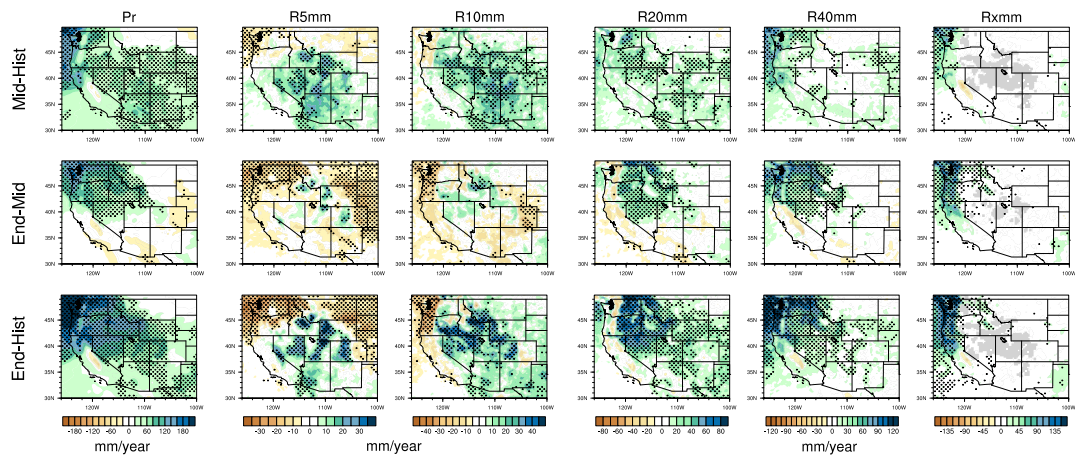
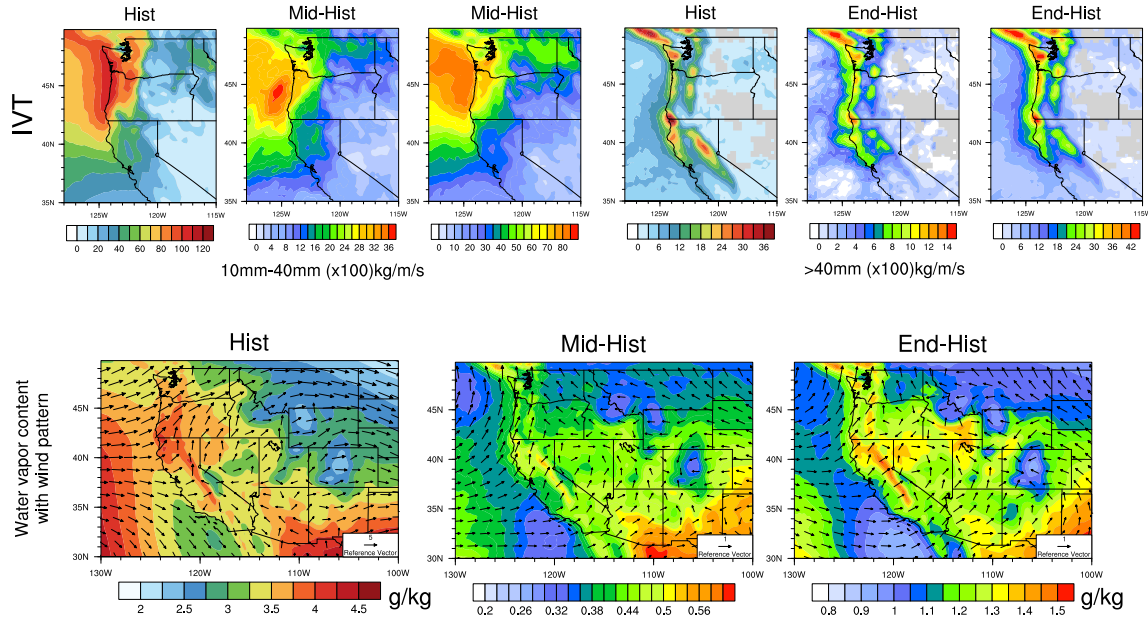


FIG. 6. Differences of precipitation behaviors from past to future over WUS averaged of each time period.
 (Note: Grids with statistically significance difference are marked with stippling.)



831 FIG. 7. Differences of precipitation behaviors from past to future over WUS averaged of each time period
 832 (continued).



833 FIG. 8. Changes of specific humidity and horizontal wind pattern at 850hPa for moisture flux illustration,
 834 and IVT for simulations under different time period of wet season (October to March) averaged over 26 years.
 835 (Note: The minimum wind vector is set to be 0.5 m/s, therefore, the wind less than 0.5 m/s is also plotted at the
 836 minimum length for better visualization.) **Specific humidity and wind pattern are averaged over all days over**
 837 **cool season rather than days with $\text{Pr}_t > 10\text{mm}$.**

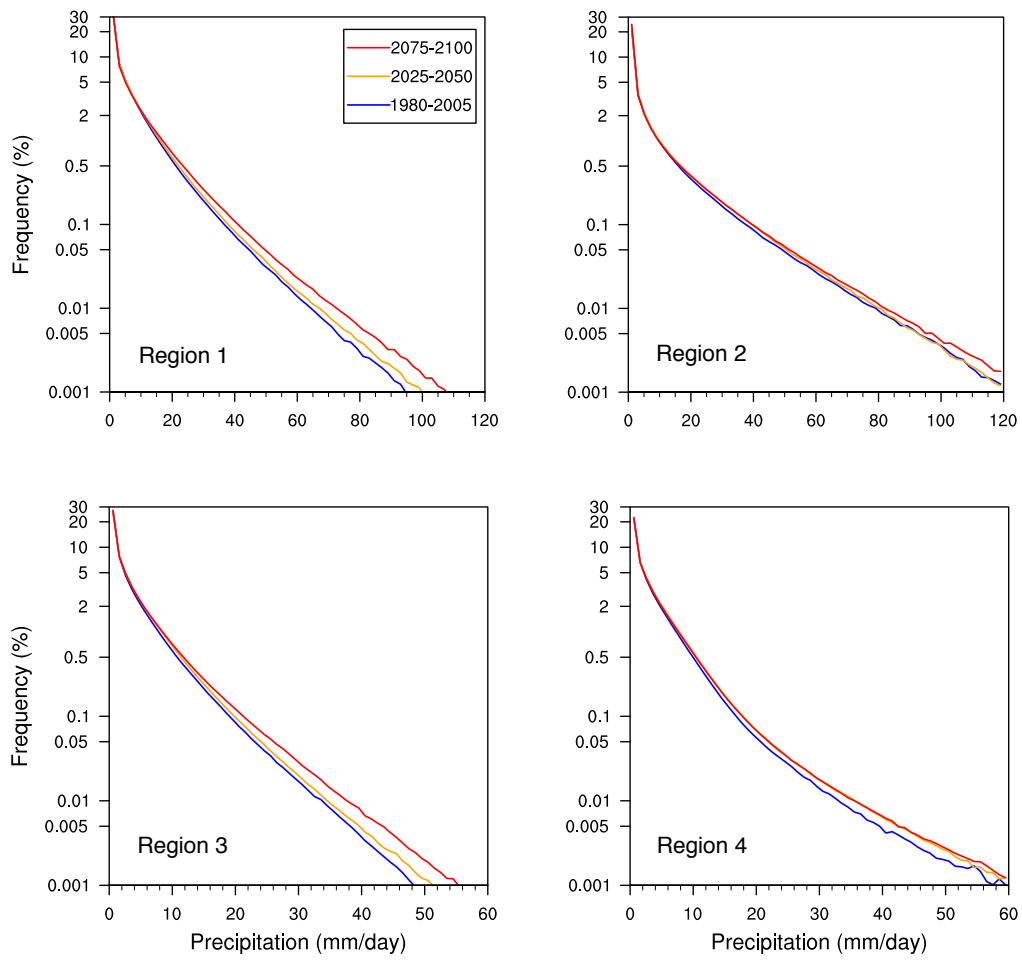
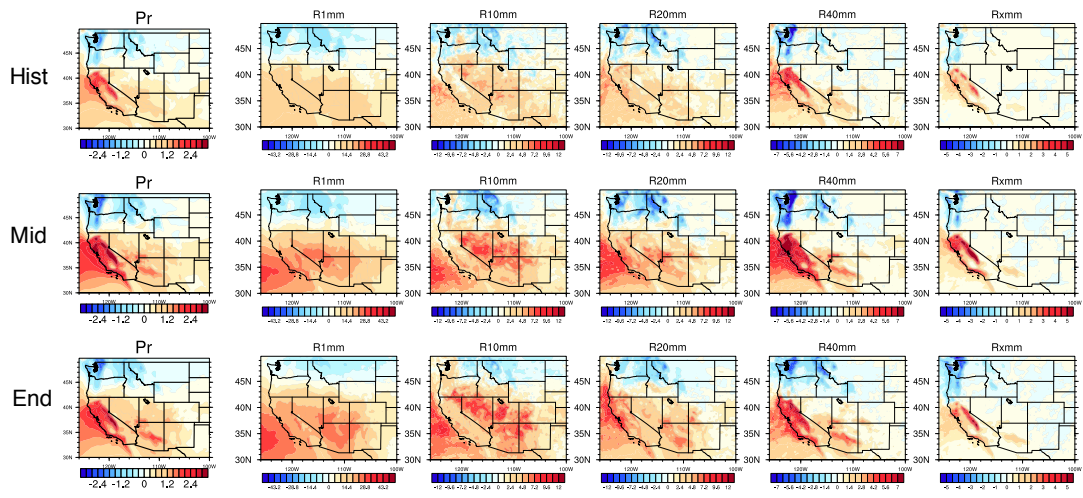
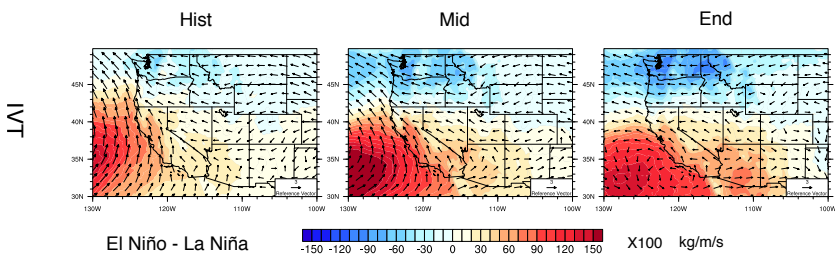


FIG. 9. Frequency distribution of rainy days ($Pr \geq 0.1 \text{ mm/day}$) over the three time periods from simulations in four regions (with logarithmic vertical scale). (Note: Region 1 to 4 cover Washington and Oregon; California; Nevada, Utah and Idaho; Arizona and New Mexico, respectively.)



841 FIG. 10. Difference of precipitation behaviors between warm and cool phases of ENSO from past to future
 842 over WUS averaged of each time period.



843 FIG. 11. Changes of IVT for simulations under different phases of ENSO of wet season (October to March).
 844 (Note: The minimum wind vector is set to be 0.5 m/s, therefore, the wind less than 0.5 m/s is also plotted at the
 845 minimum length for better visualization.)